Short Wavelength Laboratory Sources

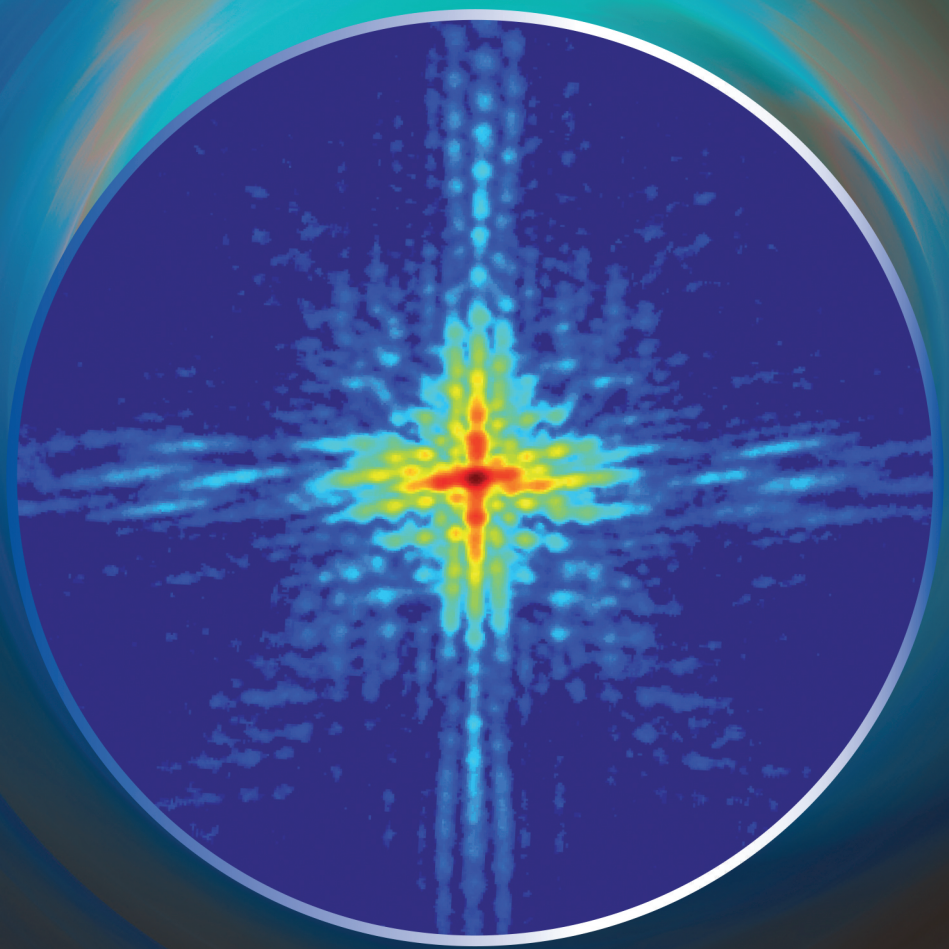

Edited by
Davide Bleiner, John Costello, Francois De Dortan,
Gerry O'Sullivan, Ladislav Pina, and Alan Michette

ROYAL SOCIETY OF CHEMISTRY

cost
EUROPEAN COOPERATION
IN SCIENCE AND TECHNOLOGY

Short Wavelength Laboratory Sources
Principles and Practices

Short Wavelength Laboratory Sources
Principles and Practices

Edited by

Davide Bleiner
University of Bern, Bern, Switzerland
Email: davide.bleiner@iap.unibe.ch

John Costello
Dublin City University, Dublin, Ireland

Francois de Dortan
Academy of Sciences of the Czech Republic, Prague, Czech Republic

Gerry O'Sullivan
University College Dublin, Dublin, Ireland

Ladislav Pina
Czech Technical University, Prague, Czech Republic

and

Alan Michette
Kings College London, London, UK

This work is a publication of the COST Action Group MP0601.

Print ISBN: 978-1-84973-456-1
PDF eISBN: 978-1-84973-501-8

A catalogue record for this book is available from the British Library

Published by The Royal Society of Chemistry,
Thomas Graham House, Science Park, Milton Road,
Cambridge CB4 0WF, UK

Registered Charity Number 207890

Visit our website at www.rsc.org/books

Printed in the United Kingdom by CPI Group (UK) Ltd, Croydon, CR0 4YY

ESF provides the COST Office through an EC contract

COST is supported by the EU RTD Framework programme

COST – the acronym for European Cooperation in Science and Technology- is the oldest and widest European intergovernmental network for cooperation in research. Established by the Ministerial Conference in November 1971, COST is presently used by the scientific communities of 36 European countries to cooperate in common research projects supported by national funds.

The funds provided by COST - less than 1% of the total value of the projects - support the COST cooperation networks (COST Actions) through which, with EUR 30 million per year, more than 30 000 European scientists are involved in research having a total value which exceeds EUR 2 billion per year. This is the financial worth of the European added value which COST achieves.

A "bottom up approach" (the initiative of launching a COST Action comes from the European scientists themselves), "à la carte participation" (only countries interested in the Action participate), "equality of access" (participation is open also to the scientific communities of countries not belonging to the European Union) and "flexible structure" (easy implementation and light management of the research initiatives) are the main characteristics of COST.

As precursor of advanced multidisciplinary research COST has a very important role for the realisation of the European Research Area (ERA) anticipating and complementing the activities of the Framework Programmes, constituting a "bridge" towards the scientific communities of emerging countries, increasing the mobility of researchers across Europe and fostering the establishment of "Networks of Excellence" in many key scientific domains such as: Biomedicine and Molecular Biosciences; Food and Agriculture; Forests, their Products and Services; Materials, Physical and Nanosciences; Chemistry and Molecular Sciences and Technologies; Earth System Science and Environmental Management; Information and Communication Technologies; Transport and Urban Development; Individuals, Societies, Cultures and Health. It covers basic and more applied research and also addresses issues of pre-normative nature or of societal importance. For more information the web address is: http://www.cost.eu

This publication is supported by COST.

PREFACE

Alan knew that: *Verba volant, scripta manent*. Spoken words fly away, written ones remain. The strength of a networking instrument, it is a bit its weakness: rapid verbal exchanges may indeed fly away. Frequently meetings with community peers, for exchanging results, problems, solutions, and research priorities established our European identity in science and technology. Especially for young researchers, or research groups without large budgets for regularly attending all the big overseas conferences, COST Actions offer a unique possibility. Support to "fly around" words (and thoughts) all over the continent, through non-archival, non-formal, non-hierarchic exchanges is great idea. The risk is however there, that when the curtain draws only a sequence of stimulating presentations and coffee breaks was made, no major legacy or touchable deliverable being left. Alan knew that.

So what? Indeed answering the "*so-what*" question is the necessary conclusion of any intellectual process. Indeed, answering the "*so-what*" question means sharp-focusing all achievements black-on-white. Alan knew that, too.

I admit it, the outfit of the present monograph has changed as Alan's commitment is irreplaceable. The original idea, as proposed by the Action's father, Prof. Alan Michette of King's College *(the place where the father of electromagnetic theory, J.C. Maxwell, was active long before Alan*), was to release a textbook. After he passed away in May 2013, the big endeavor that relied fully on his shoulders faced a stall. Thus, I have more modestly offered my service to nail down available contributions for *words to remain*. Alan would expect that. However less ambitious my service has been.

Finally, we have edited an excellent collection of thematic contributions, providing state-of-art updates as well as a complete vision on the field of short-wavelength laboratory sources. The ongoing follow-up Action MP1203, led by Dr. Philippe Zeitoun, can now build-up on solid bases. We did not let any spoken work fly away. *Alan knew that.*

Davide Bleiner
Bern

This book is dedicated to the memory of Prof. Alan Michette, who sadly passed away in 2013 before this book was finished.

THE COST ACTION MP0601 – Short Wavelength Laboratory Sources

It was in September 2006 in Pisa, the city of the leaning tower, that the proposal for the COST Action MP0601 took its final shape and became a reference framework for the community of short wavelength radiation science and technology. It was in that occasion that Alan Michette was unanimously asked to lead what was going to become a truly comprehensive and uniquely effective initiative in a rapidly evolving scientific field.

Pre-Action meeting in Pisa, 4-5 September 2006

Short wavelength radiation has been used in medicine and materials studies since immediately after the 1895 discovery of x-rays. The development of synchrotron sources over the last 25 years, or so, has led to a boom in applications in other areas. More recently, the advent of X-ray free electron lasers is opening new horizons in the exploration of matter.

However, besides the large capital investments required for these large installations (more than 100M€ to build, perhaps about 1M€ per beam-line per year to run), synchrotron beam-lines are often over-subscribed by factors of three or more. Despite the widely-acknowledged advantages of synchrotron radiation, many opportunities offered by X-rays are hindered by the scale of the installation and by the impossibility to conceive a large scale use of synchrotron radiation.

Indeed there is much work, of great economic, societal or health significance, that can never be done using synchrotron sources. An example is the possibility offered by synchrotron radiation in medical diagnostic imaging which, however, will never become routine at the present level of size and cost. Security inspections at airports and ports – as these inevitably become more extensive, and sophisticated, throughput must be increased significantly to minimize delays. In-field studies of valuable items that cannot be transported to synchrotrons, require the development of compact integrated (source, optics, detector) systems. At the same time, in-field studies of pollutants *in situ*, require similar development of integrated systems but probably at different energies, not to mention routine medical and dental work, where improved sources and associated equipment will lead to reductions in patient dose. Some applications also need continuous, high throughput, like EUV lithography, for future generation micro/nano circuits or radiobiological studies of radiation-induced mutations, just to mention a few.

According to the Web of Science, since 1990 the total number of scientific papers per year has risen by 45%, while there has been an eleven-fold increase in publications concerning X-rays. Over the same period there has been a 30 times increase in papers involving synchrotron sources, but even so fewer than 7% of x-ray applications use synchrotrons.

zAll the above point to the need to develop alternative, cost effective, more accessible sources which can offer at least some of the properties of synchrotrons. This was only the underlying background motivation for starting the Action that was then conceived with a range of objectives to cover all aspects of short wavelength radiation science and technology.

6th Joint Working Groups Meeting in Kraków, 27-28 May 2010

Indeed, in Alan's vision, shared by all participants, the Action's underlying aim was to maintain and enhance Europe's position in the increasingly important research area of short wavelength radiation, in order to widen access to applications that either can only currently be undertaken at large scale facilities such as synchrotrons or cannot be done at such facilities. Applications that will be enhanced include medicine (such as studies related to radiation-induced cancers), materials science, security, environmental science, lithography and chemical analysis. An example of the latter is in determining the chemical constitution of paints for restorative work and other aspects related to cultural heritage and historic artefacts. The wavelength range is natural for nanoscience and nanotechnology and thus there will be significant impact for the development of nanoscale structures and investigations. Similarly, the wavelength range is suitable for nanoscale imaging of specimens in near-natural environments. It has also been demonstrated that short wavelength spectroscopy provides improved detection limits for impurity concentration measurements in metals and alloys.

1st Joint Working Groups Meeting in Pisa, 22-23 November 2007 .

In order to realize the main purpose, the Action was structured to address several secondary objectives that were recognized as crucial in the development if the field. Of paramount importance was the need to increase output fluxes by at least an order of magnitude over existing values, both spectrally integrated and at specific, application dependent, wavelengths. Here a reference application that would benefit from increased flux was identified as short wavelength lithography, throughput being an essential user requirement. Parallel to this, source size was also identified as a fundamental parameter to control. Indeed, applications such as high-resolution (scanning) microscopy and radiobiological probing of cells and sub-cellular structures require small source sizes, typically below 1μm, without compromising flux. This means achieving sources with high brightness and, where possible, collimated emission. In the case of electron impact and similar sources where the primary beams are continuous in time, the above requirements also call for alleviation of target heat loading. Instead, in the case of plasma sources, tipically pulsed, flux increase will require higher repetition and, inevitably, new ways of replenishing the material from which the plasma is formed, the so-called targetry requirements. Wide ranges of target materials and geometries – solid, layered, gaseous, liquid – are possible in plasma sources and, as discussed here, the Action addressed much of this complexity to provide reliable and dependable solutions taking into account parameters such as flux, spectral power density, pulse duration and debris.

4th Joint Working Groups Meeting in Salamanca, 14-15 May 2009 (right)

Another main objective of the Action concerned the sources of ultrashort X-ray pulses. Indeed, a dramatic development in ultrashort-pulse laser-driven X-ray sources was occurring when drafting the programme of the Action and such sources were becoming increasingly important and likely to open new dimensions in research and applications.

Although some developments in short pulse sources will remain facility based, laboratory scale sources are invaluable as test beds for optics (especially non-dispersive), detectors, methodologies (e.g., pump-probe experiments), instrumentation, etc., before much more expensive tests at large-scale sources, and the Action took care of this scenario.
The development of improved compact portable sources was and remains an increasingly strategic objective for development of sources for a variety of applications. Carbon nanotube cathodes, with integrated optics and detectors, may offer efficient in-field measurements for environmental and heritage conservation applications. However, miniaturization of sources based upon other concepts, including laser-driven sources, may soon became a reality and the Action explored underlying principles of these sources to spot bottlenecks and possible solutions.
An aspect of great relevance is the use of focusing optics to collect, manipulate and focus radiation. This is a wide field of research itself and the Action did not neglect the importance of focusing techniques while still retaining the main emphasis of sources.
Finally, significant attention was dedicated to the ongoing effort in generating dependable modeling resources that can drive experimental programmes and establish robust methods of comparing source behaviour with respect to variable parameters.
All this and much more was in the DNA of the Action and was pursued in a friendly environment, by a collective effort involving enthusiastic young researchers, motivated group leaders and distinguished senior scientists, all guided and inspired by our friend Alan.

Alan Michette, Coordinator of the Action

Leonida A. Gizzi
(vice-chair of the Action)

Contents

Modelling and Simulation

Source Development

Integrated Systems

Applications

Modelling and Simulation

ATOMIC AND PLASMA PHYSICS SOFTWARE AND DATABASES FOR THE SIMULATION OF SHORT WAVELENGTH SOURCES

F. de Dortan, [1,2] D. Kilbane, [3] J. Vyskočil, [4] P. Zeitoun, [5] A. Gonzalez, [2] A. de la Varga, [2] O. Guilbaud, [6] D. Portillo, [2] M. Cotelo, [2] A. Barbas[2] and P. Velarde[2]

[1]Institute of Physics, Academy of Sciences of the Czech Republic, Prague, Czech Republic
[2]Institute of Nuclear Fusion, UPM, Madrid, Spain
[3]University College Dublin, Belfield, Dublin 4, Ireland
[4]Czech Technical University, Prague, Czech Republic
[5]Laboratoire d′Optique Appliquée, ENSTA ParisTech, Chemin de la huniere, 91671 Palaiseau, France
[6]Laboratoire de Physique des Gaz et des Plasmas, Universite Paris XI, 91761 Orsay, France

1 INTRODUCTION

A large variety of software has been developed for numerical simulations of plasma radiation emission and transport and the design of optics. Many of these codes are not specifically for short wavelengths but they can be helpful in the design of X-ray and extreme ultraviolet (XUV) sources. The astrophysics community has written codes to study the spectra and evolution of stars and gas clouds while civilian and military applicants of atomic processes were aware very early of the need for atomic, plasma and hydrodynamic software to simulate nuclear fission and fusion and their effects. Of more relevance to low cost EUV sources, the large synchrotron community has also generated efficient tools for the simulation of radiation from electrons and the design of short wavelength optics.

The present intention is not to present all the available software, since resources such as Computer Physics Communications[1] and Plasma Gate[2] give much more comprehensive, if never complete, reviews. Instead, some of the more popular programs will be introduced, as they are proven and tested assistance is available from experienced users. The software may be downloaded from the web sites listed in the references; registration is sometimes required.

2 DATABASES

The National Institute of Standards and Technology (NIST) Atomic Spectra Database is a comprehensive compilation of the experimental wavelength, strengths and level energies of spectral lines with links to the original papers.[3] Access to the ionisation energies is available on the same website. The Atomic Molecular Data Service (AMDAS) of the International Atomic Energy Agency (IAEA) is another source of databases and online software.[4]

The OPAL opacity tables[5,6,7] give access to the monochromatic Rosseland opacities of 22 elements of interest for solar astrophysics - hydrogen, helium, carbon, nitrogen, oxygen, fluorine, neon, sodium, magnesium, aluminium, silicon, phosphorous, sulphur, chlorine, argon, potassium, calcium, titanium, chromium, manganese, iron and nickel. The opacities

are for solar mixtures but may be easily extended to other mixtures and pure elements. Local Thermodynamic Equilibrium (LTE) is assumed. Some equations of state are also available for the most representative elements of the Sun, namely hydrogen, helium, carbon, oxygen and neon. Some Fortran subroutines are available for interpolation. The tables are computed and maintained at the Lawrence Livermore National Laboratory.[8]

The Opacity and Iron[9,10] Projects are international collaborations to estimate stellar envelope opacities and compute Rosseland mean opacities of elements relevant for astrophysics, essentially the same list as OPAL except for helium, fluorine, phosphorous, potassium and titanium. Data tables can be generated online choosing custom mixture of elements. A global archive can also be downloaded including some routines to compute the opacities online; radiative accelerations are also included. Fine structure atomic data - energy levels, radiative transition probabilities, electron impact excitation cross sections and rates and photo-ionisation cross sections - are also available online.[11,12]

Sesame[13] is a library of tables for the thermodynamic, electric and radiative properties of materials with Fortran subroutines for the use of the libraries, three of which are available:

- Equation Of State (EOS) for over 150 materials (simple elements, compounds, metals, minerals, polymers, mixtures...). This library contains pressure, energy, Helmholtz free energy, thermal electronic and ionic contributions, and sometimes vaporisation, melt and shear tables for temperatures in the range 0-105 eV and densities of 10^{-6} - 10^{4} g/cm^3;
- An opacity library where mean Planck and Rosseland opacities as well as ionisation and electron conductive opacities are provided for temperatures above 1eV and for elements with Z=1-30;
- A conductivity library giving mean ionisation, electrical and thermal conductivities, thermoelectric coefficients and electron conductive opacities for elements with Z=1-96.

Many methods are used to obtain the EOS, the aim being to have thermodynamically self-consistent equations that are generated using the most accurate physics to provide the best possible agreement with available experimental data. Fortran subroutines are provided to read the data and compute the thermodynamic variables and their first derivatives at the desired points. Libraries are created and maintained at the Los Alamos National Laboratories where they can be obtained after registration.[14]

3 ONLINE SOFTWARE

The COWAN[15] suite of code on the Los Alamos T4 network[16] gives direct access to the computation of detailed or averaged energy levels including configuration interactions. It is based on the Hartree Fock method,[17,18] and line strength, collisional excitation in distorted waves (DW) or the first order many body theory (FOMBPT) approximations are also available. Collisional ionisation can be computed using the scaled hydrogenic,[19] binary encounter[20] (billiard-like collision taking into account target momentum) or distorted wave[21] approximations. Photo-ionisation cross sections as well as auto-ionisation rates are also calculated.

A web interface of the FLYCHK code[22], is available at the National Institute of Standards and Technologies (NIST). It generates atomic level populations and charge state distribution as well as overall radiative losses for low- to mid-Z elements under non-LTE

conditions. The full version of this code, which is discussed more fully in section 3.3, is available to download.[23,24]

The Centre for X-Ray Optics (CXRO) at the Lawrence Berkeley National Laboratory provides online access to the computation of transmission factors of neutral materials (either gaseous or solids, and pure or compounds).[25] It is also possible to load the scattering factor tables in order to create custom databases for local calculations. It is also possible to compute online the reflectivities of materials or multilayers, whatever the composition and density. Transmission gratings efficiency can also be calculated.[26]

4 SOFTWARE TO BE DOWNLOADED OR REQUESTED

4.1 Software for Atomic physics

Multi Configuration Hartree Fock (MCHF) codes were initially developed by Charlotte Froese Fischer.[27] Many versions are available on the Computer Physics Communications (CPC) Program Library[28] and on the internet to compute structure, wave functions and energy levels as well as radiative transition rates. Many subsequent programs are also available to determine the collisional rates between the computed levels within a wide range of approximations, for example ATSP2K on CPC or at NIST.[29]

Single or Multi Configuration Dirac Fock (SCDF[30], MCDF[31,29]) codes rely on the fully relativistic Dirac equation. Many versions exist, all permitting structural computation with level energies and radiative transition rates. Some also give access to collisional transition and photo-ionisation cross sections and auto-ionisation rates within the same package; otherwise external programs have to be used subsequently. Many of these present multiple optimisation procedures to increase the precision of the energies and wave-functions or rates useful for extremely detailed spectroscopy. This may not be useful for sources emitting many closely spaced lines but may help describe better X-ray laser amplification of single lines. The Multi Configuration Dirac Fock and General Matrix Element (MCDFGME)[32] package is more complete, including Born collisional excitation, photo-ionisation and auto-ionisation cross sections and rates.

Autostructure[33,34] is a Fortran program for computing atomic and ion energy levels, radiative and auto-ionisation rates and photo-ionisation cross sections. It is based on Superstructure[35] and performs calculations in orbital angular momentum / spin (Russell Saunders or LS-) or intermediate (jj-) coupling[36] using non-relativistic or semi-relativistic wave-functions. Radial functions use a model potential, either Thomas-Fermi (TF) or Slater-Type-Orbital (STO). The data can be post processed to generate di-electronic recombination rate coefficients for doubly excited state populations and satellite line emission modelling. This code has been used successfully to model di-electronic recombination of tin ions relevant to EUV lithography.[37]

The COWAN[15,38,39] suite of Fortran 77 codes is a package of computer programs using the MCHF method to compute level energies and structures, radiative transition wavelengths and probabilities, electron impact excitation, photo-ionisation cross sections and auto-ionisation rates. It provides full access to all the intermediate information and variables such as radial wave-functions, centre of gravity configuration energies, radial Coulomb and spin-orbit integrals. It is also possible to perform least squares fits to experimental energy levels for spectroscopic use.

The Relativistic Atomic Transition and Ionization Properties (RATIP)[40] suite of programs calculates relativistic atomic transition, ionization and recombination properties. It is particularly suitable for open-shell atoms and ions and is capable of calculating energy

levels, transition probabilities, Auger parameters, photo-ionisation cross sections and angular parameters, radiative and di-electronic recombination rates and many other atomic properties. It was developed as a scalar FORTRAN 90/95 code and all computations are performed within the MCDF framework as implemented in GRASP92 and GRASP2K packages[41,42]. Successful applications of RATIP include atomic photo-ionisation and electron spectroscopy, study of highly charged ions,[43] spectroscopy of heavy and super-heavy elements,[44] the generation of atomic data for astrophysics and plasma physics[45] and the search for time reversal violating interactions in atomic systems.[46]

The Hebrew University – Lawrence Livermore Atomic Code (HULLAC)[47,48] is a complete suite of Fortran atomic codes including structure and transitions. It is a consistent atomic model using the same wave functions for computing all atomic processes relevant to plasma spectroscopy. These wave functions are obtained by solving the Dirac equation in a parametric potential. A factorisation /interpolation method allows faster computation of collisional cross sections. The initial version of the code has been recently rewritten to increase the size of matrices and allow not only detailed levels but also configuration averaging both relativistic and non-relativistic. It now has easy user input, a collisional radiative solver, the ability to use the mixed transition arrays and to model the effects of external radiation fields; spectral software is also included. HULLAC is being used by many groups around the world and may be obtained from its authors.

The Flexible Atomic Code (FAC)[49,50] is a complete suite of atomic codes including structure and transitions, mostly similar to HULLAC. It solves the relativistic Dirac equation, using a single central parametric potential to compute the orbitals. Radiative decay, collisional excitation and ionisation, auto-ionisation and photo-ionisation cross sections and rates are computed within the distorted wave approximation. Coulomb Born approximation with exchange (between incoming and target electrons) and binary encounter dipole[20] approximations can also be used to compute the collisional ionisation more quickly. Results can be either detailed or averaged in relativistic configurations. Detailed levels may also be split into magnetic sublevels and the transitions computed between these. FAC is written in FORTRAN 77 for the physics and C for the architecture. Two interfaces are available, one online, the other a PYHTON scripting interface which allows easier extensive use of the program. It is very stable and straightforward to install. A collisional radiative solver and spectrum computation are available but not documented and difficult to use and so most users develop their own solver and radiative emission and transmission software.

4.2 Equation of State and Opacities

ABINIT[51,52] is a widely used package allowing to compute the total energies, charge densities and electronic structures of a combination of a nucleus and electrons using density functional theory (DFT). ABINIT also include options to optimise the geometry according to the DFT forces and stresses, to perform molecular dynamics simulations using these forces, or to generate dynamical properties (vibrations and phonons), dielectric properties, mechanical properties and thermodynamic properties. Some possibilities of ABINIT go beyond DFT, for example the many-body perturbation theory, which uses the single particle Green´s function G and the screened Coulomb interaction W (GW approximation), and Time-Dependent DFT. The codes have been written in Fortran 90 by more than 200 developers who upgrade and maintain it under the GNU/GPL license.

IONMIX,[53] a Fortran 77 code available on the CPC website[28] for determining the EOS and radiative properties of LTE and non-LTE plasmas composed of many different elements, is designed for plasmas with high electron temperatures, $T_e \geq 1eV$, and low to

moderate ion densities $N_i(cm^3) \leq 10^{20}(T_e/Z)^3$. Steady-state ionisation and excitation populations are determined by either the Saha-Boltzmann equation or by collisional radiative resolution using hydrogenic ion approximation. Bound-bound, bound-free, free-free and electron scattering processes are taken into account to compute multi-group Planck and Rosseland mean opacities. Auto-ionisation and reverse process are not taken into account.

BADGER[54] is an EOS library written in Fortran 90 and available on the CPC website.[28] It models plasmas more correctly in the low temperature, high density regime, especially inertial confinement plasmas. It computes single or double (different electronic and ionic) temperatures plasmas using the Thomas Fermi model.[56] Ion EOS data, for Z=1-86, is obtained either from the ideal gas model or from a quotidian EOS (semi-empirical fitting of available experimental data for higher densities and lower temperatures) with scaled binding energies.[55] Electron EOS data may be computed from the ideal gas model or from an adaptation of the screened hydrogenic model with angular momentum splitting.[57] The ionisation and EOS calculations can be carried out assuming LTE or non-LTE mode using a variant of the Busquet equivalent temperature method.[58] The code is written as a software library to be directly linked to external codes without having to generate tabular data. It also includes a wrapper code that allows the generation of data tables if in-line implementation is impractical.

4.3 Computation of Synthetic Spectra and Spectroscopic Analysis

Cretin[59,61] is a multi-dimensional non-LTE radiation transfer code. It combines atomic kinetics and radiation transport in a self-consistent way and is suitable for modelling laboratory plasmas with a wide range of applications, including non-uniform materials, complex geometries (planar, cylindrical and spherical in 1D, Cartesian and cylindrical in 2D, Cartesian in 3D) and non-negligible optical depths. Atomic data is generated externally for Cretin using either average atom or unresolved transition arrays (UTA) models for applications that focus on gross energetics, or fully detailed models such as the flexible atomic code (FAC)[49] when spectroscopic comparisons are required. Cretin has been successfully applied in a variety of applications including inertial confinement fusion (ICF), magnetic fusion, X-ray lasers and laser produced plasmas. Recently it was successfully applied to match experimental data for laser-driven systems and hohlraums.[60]

FLYCHK,[22,23] as briefly described above, is a straightforward and rapid tool which provides ionization and population distributions of homogeneous plasmas with accuracy sufficient for most initial estimates; in many cases is applicable for more sophisticated analysis. FLYCHK solves rate equations for level population distributions by considering collisional and radiative atomic processes. The code is designed to be straightforward to use and yet is general enough to apply for most laboratory plasmas. It can also be applied to low-to-high *Z* ions in either steady-state or time-dependent situations. Plasmas with arbitrary electron energy distributions and single or multiple electron temperatures can be studied as well as radiation-driven plasmas. To achieve this versatility and accuracy in a code that provides rapid response schematic atomic structures are used, such as scaled hydrogenic cross-sections and look-up tables. The code also employs the *jj* configuration averaged atomic states and oscillator strengths calculated using the Dirac–Hartree–Slater model[62] for spectrum synthesis. Numerous experimental and analytic comparisons performed have shown that FLYCHK provides meaningful estimates of ionization distributions, well within a charge state for most laboratory applications.

PRISM-SPECT[63,64] is a commercial spectral analysis code, designed to simulate the atomic and radiative properties of laboratory and astrophysical plasmas. For user specified

thermodynamic conditions, it computes emission, absorption and ionisation of LTE and non-LTE plasmas. Population and spectra can also depend on an external radiation field and non-Maxwellian electron distributions. The resolution can be either stationary or time-dependent. A strong emphasis has been put on a graphic package to help in setting up the problem, visualizing the results, the progress of computations and spectroscopic analysis. All the elementary atomic processes and their reverses are taken into account. Doppler, natural, auto-ionisation, collisional electronic- and ionic- Stark broadening are employed to compute the line profile. Experimental energy levels and oscillator strength are used when available. An atomic database for elements Z=1-18 is included; other elements may be obtained on request.[64]

4.4 Radiative Hydrodynamics

MEDUSA[65] is a one dimensional Lagrangian radiation hydrodynamics code, developed for simulations of laser inertial fusion. Electrons and ions are treated as having different temperatures but behaving as perfect gases. Radiative losses are through Bremsstrahlung only. Thermonuclear reactions are included in the computation and different ion species may be specified at the same time. The geometry can be planar, cylindrical or spherical. The code is written in standard Fortran (64) and is available from CPC.[28]

MULTI[66,67] is a one dimensional Lagrangian radiation hydrodynamics code also available from CPC. It was developed for inertial confinement fusion and related laser experiments. The hydrodynamic equations are combined with a multigroup method for radiation transport. It uses external tables for EOS data, Planck and Rosseland opacities. The original geometry was planar, but a large community of users has improved it and versions with femtosecond laser interactions, cylindrical and spherical geometries have been implemented. It is written in Fortran 77 and R94 (a language developed for easier interfacing and translated to C).MULTI 2D[67,68] is a two dimensional version designed for indirect inertial fusion applications and diagnosis of experiments. The geometry is cylindrical and hydrodynamics is Lagrangian. EOS and opacities are interpolated from external tables. It is written in C and is available from CPC.[28]

Z*BME (Z* Blackbox Modelling Engine)[69] is a commercial system tool based on the adaptation of the two dimensional radiation-magneto-hydrodynamic code Z*[69] to facilitate numerical modelling of EUV plasma sources by non-specialists. It can simulate both discharge and laser produced plasma sources and generate two dimensional maps of thermodynamic conditions of the plasma as well as ionisation maps, radiative losses, conversion efficiency maps and time-dependent limited bandwidth EUV emission power. An imbedded particle in cell (PIC) code provides time dependent fast ion production maps. It includes its own tables for thermodynamic equilibrium properties (EOS, ionisation) and radiative properties. Non-LTE ionisation and radiation transport can also be computed. At the end of simulations, spectra and heat fluxes can also be output. It is integrated into a specific computation environment to provide a turn-key simulation instrument without specialist knowledge in numerical simulation; thus Z*BME is used in many laboratories. Numerous simulations have been conducted to simulate EUV sources for nanolithography, describing, for example, debris production from laser interactions with mass limited droplets, conversion efficiency of xenon and tin based plasma sources, thermal load of discharge source electrodes and non-stationary and non-LTE effects on plasma ionisation. The code is available from EPPRA sas (Villebon sur Yvette, France)

ARWEN[70] is a two dimensional hydro-radiative code with adaptive mesh refinement (AMR) including laser interactions. It is an Eulerian code with flux limited electron thermal conduction and multiple groups of photon frequencies (multigroup) radiation

transport. It uses external data files for EOS and multigroup opacities. Laser energy deposition can be treated with a simple model or assuming refraction effects with a 2D ray-tracing subroutine. It includes two temperatures (electron and ion), time-dependent ionisation and gain computation. Planar and cylindrical geometries are available. The AMR allows the resolution to increase only in regions where the gradients increase over a defined limit and leads to uniform numerical errors while saving computation time. A graphical interface is included to display 2D time-dependent results as videos and a standard interface in hierarchical data format (HDF) is also available for easy post-processing by other codes. ARWEN is written in Fortran and C++ and is available from Pedro Velarde (DENIM/UPM, Madrid).

4.5 X-ray Lasers Hydrodynamics and Output

EHYBRID[71] is a 1.5 dimensional (one dimensional plus autosimilar expansion in transverse direction) hydroradiative Fortran code coupled with level population dynamics, able to model X-ray lasers dynamics. It provides extensive information about the plasma dynamics and the gain of the modelled X-ray laser. Non-normal incidence of the pumping laser pulse can be taken into account as well as very short laser pumping pulses. It uses external EOS files or a perfect gas approximation if EOS is not available. It also uses external atomic data files to compute the transient ionisation and the evolution of lasing populations. EHYBRID is available from Geoffrey Pert (York University, UK)

4.6 High Harmonic Generation

QPROP[72,73] is a time-dependent Schrödinger (or Kohn-Sham) solver, designed for the study of atoms or other spherical systems in intense laser fields. It was developed to study laser-atom interactions in the non-perturbative regime where non-linear phenomena such as above-threshold ionisation, high-harmonic generation and dynamic stabilisation occur. Two methods of resolution are available : full resolution with density functional theory[74] (DFT, also called Kohn-Sham equations) where the number of perturbed electrons is chosen by the user or faster but limited resolution with a "frozen core" of electrons simulated by an external potential a single-active (perturbed) electron. In DFT, wave functions are expanded in spherical harmonics. The time-dependent Schrodinger equations can only be solved for a linear laser field polarisation. In the single-active non-relativistic approximation, the time-dependent Schrodinger equation is solved in three dimensions and the laser polarisation can be either linear or elliptical. The emitted photon spectrum is obtained by Fourier-transformation of the dipole acceleration. QPROP is written in C++ and maintained at Rostock University.

4.7 Plasma Physics (PIC codes)

LPIC++[75,76] is a one dimensional electromagnetic and relativistic particle in cell (PIC) code for simulating highly intense and ultra-short laser-plasma interactions, including ionization dynamics and collisions. It is written in C++ and is designed to work on Linux-Unix type parallel architectures and has been extended to include radiation friction force effects using Landau-Lifschitz approximation.[77] A 2D version is also available.

EPOCH[78,79] is a multidimensional (1D, 2D, 3D) PIC code for general plasma simulations. It is an electromagnetic relativistic code which features arbitrary laser pulse and plasma slab shapes, higher-order particle shapes, and a moving window algorithm for simulating large domains. It includes Monte Carlo algorithm for simulation of quantum

electrodynamic (QED) effects at ultrahigh intensities such as emission of gamma-rays and electron-positron pair creation. It has a rich set of output options, with provisions for visualization in Matlab, VisIt and IDL. The code is written in Fortran 90 and parallelised using the MPI library. Input is specified with text files.

4.8 Propagation of X-ray Lasers and the Effect of Coherent X-rays on Materials

The free electron laser atomic, molecular, and optical physics program package FELLA[80,81] is a suite of codes to study the interaction of optical laser radiation and X-rays with atoms and molecules, to explore the ultrafast and the ultra-small. The motivation was to study atoms and molecules using X-ray free electron lasers (XFEL) in combination with intense optical lasers. It can be used in more general cases such as interaction induced by intense synchrotron radiation. The atomic physics program treats the electron structure of atoms in Hartree-Fock-Slater approximation and their interaction with photons of one or two energies. The molecular physics programs treat the X-ray absorption by laser-aligned molecule and the optical physics code computes the propagation of laser and X-rays through gaseous media. FELLA is written in Fortran 95 and maintained at Argonne National Laboratory.

4.9 Optics Design

IMD[82,83] is an IDL application which can calculate specular and non-specular (diffuse) X-ray to infrared performances of an arbitrary multilayer structure, i.e., a structure consisting of any number of layers, any thickness and any materials. Reflectance, transmittance, absorbance, electric field intensities, phase shifts as well as the amplitude and phase components of the reflectance (psi and delta functions) for ellipsometry are computed with an algorithm which includes interfacial roughness and diffusion. A stochastic model of film growth and erosion can be used to account for the evolution of interfacial roughness through the film stack. Specular and non-specular optical functions can be calculated as functions of incidence angle, wavelength, polarisation, spectral and angular resolution, as well as parameters that describe the multilayer structure. It includes a database of optical constants for over 150 materials but also allows material constants to be input. IMD uses a simplified graphical interface to help define the properties of the multilayers and also to visualise and analyse in 1D or 2D the properties of the designed optic.

ZEMAX[84] is a commercial optical design program. It is widely used to design and analyse optical systems performing sequential ray tracing through optical elements, non sequential ray tracing for analysis of straight light and physical optics beam propagation. It can model the propagation of rays through elements such as lenses, mirrors and diffractive optical elements. It models the effect of optical coatings and generates spot diagrams and ray-fan plots. The optics propagation feature can be used for problems where diffraction is important, including the propagation of laser beams, holography and coupling of light into single-mode optical fibres. It can be useful in optimizing performance and reducing aberrations. Although the program is designed for visible light users can specify the physical characteristics for other wavelength.

RAY[85,86] is BESSY synchrotron's ray tracing program to calculate synchrotron radiation beamlines. It is a FORTRAN design tool also for general optics applications in IR, UV, soft and hard X-rays which may work on Windows as well as Linux platforms. It can compute transmission, reflection, dispersion or diffraction as well as rocking curves, photon flux, resolving power and polarisation of/on nearly all kind of optics geometries such as zone plates, slits, foils, mirrors, spherical or planar gratings, crystals, multilayers

and graded multilayers... The code starts with a source volume with defined emission characteristics and computes its modification by optical elements, taking into account the phase space to obtain wavefront and coherence characteristics. Various orders of reflections on gratings being treated. It is designed user-friendly and easy to learn.

4.10 Image Analysis

XTRACT[87] is a suite of Windows based programs specifically designed for the reconstruction and structure recovery of samples studied by X-ray phase contrast imaging. It contains tools for pre-processing of recorded data as well as phase retrieval and cone beam computed tomography modules, software for X-ray image simulation, analysis and processing. More than 20 different algorithms are available for phase and / or amplitude extraction. It can treat most standard formats of grey-scale images and can be obtained from the Australian National Science Agency CSIRO.[88,89]

References

[1] http://www.journals.elsevier.com/computer-physics-communications/
[2] http://plasma-gate.weizmann.ac.il/directories/free-software/
[3] http://www.nist.gov/pml/data/asd.cfm
[4] http://www-amdis.iaea.org/
[5] C. A. Iglesias and F. J. Rogers, Astrophys. J. 464, 943 (1996)
[6] F. J. Rogers, F. J. Swenson, and C. A. Iglesias, Astrophys. J. 456, 902 (1996))
[7] Chen, Xue-Fei; Tout, Christopher A. Chinese J. of Astron. and Astrophys., V.7, n.2, pp. 245-250 (2007).
[8] http://opalopacity.llnl.gov/opal.html
[9] Seaton M.J., 1987, J. Phys. B 20, 6363
[10] Badnel et al., MNRAS, 360, 458 (2005))
[11] http://op-opacity.obspm.fr:8080/opacity/
[12] http://opacities.osc.edu/rmos.shtml
[13] B. I. Bennett, J. D. Johnson, G. I. Kerley, and G. T. Rood, "Recent Developments in the Sesame Equation-of-State Library," Los Alamos Scientific Laboratory report LA-7130 (1978).
[14] http://t1web.lanl.gov/doc/SESAMEdbasetxt.html.
[15] The Theory of Atomic Structure and Spectra (Los Alamos Series in Basic and Applied Sciences) Robert D. Cowan
[16] http://aphysics2.lanl.gov/tempweb/lanl/
[17] V. Fock, Z. Physik 61, 126 (1930}
[18] D. R. Hartree and W Hartree, Proc. Roy. Soc. A156, 9 (1935)
[19] R. E. H. Clarck et al, Ap. J., 381 (1991) 597
[20] L. Vriens, Phys. Rev. 141 (1966) 88 and Y.-K. Kim and M. E. Rudd, Phys. Rev. A 50 (1994) 3954
[21] I. I. Sobelman, V. A. Vainstein and E. A. Yukov, "Excitation of Atoms and Broadening of Spectral Lines", Nauka, Moscow (1979)
[22] H. K. Chung, High Energy Density Physics, 1 (2005) 3
[23] http://www-amdis.iaea.org/FLYCHK/
[24] http://nlte.nist.gov/FLY/
[25] B.L. Henke, E.M. Gullikson, and J.C. Davis. X-ray interactions: photoabsorption, scattering, transmission, and reflection at E=50-30000 eV, Z=1-92, At. Data Nucl. Data Tables Vol. 54 (no.2), 181-342 (July 1993).
[26] http://henke.lbl.gov/optical_constants/
[27] Computational Atomic Structure: An MCHF Approach, C. Froese Fischer, T. Brage, P. Jönsson (Institute of Physics, Bristol, 1997)
[28] http://cpc.cs.qub.ac.uk/

[29] http://nlte.nist.gov/MCHF/
[30] A. L. Ankudinov et al., Comput. Phys. Comm. 98 (1996) 359
[31] F. A. Parpia, C. Froese Fischer and I. P. Grant, Comput. Phys. Comm. 175 (2006) 745
[32] https://dirac.spectro.jussieu.fr/mcdf/mcdf_code/mcdfgme_accueil.html
[33] N. R. Badnell, J. Phys. B 19, 3827 (1986))
[34] http://amdpp.phys.strath.ac.uk/tamoc/
[35] W. Eissner, M. Jones and H. Nussbaumer, CPC 8, 270 (1974))
[36] W. C. Martin and W. L. Liese, "Atomic Spectroscopy", originally in chapter 10 of "Atomic, Molecular and Optical Physics Handbook, G. W. F. Drake Ed., AIP Press, Woodburry, NY (1996)
[37] N. R. Badnell, A. Foster, D. C. Griffin, D. Kilbane, M. O'Mullane and H. P. Summers, J. Phys. B: At. Mol. Opt. Phys. 44, 135201 (2011)
[38] ftp://plasma-gate.weizmann.ac.il/pub/software/dos/cowan/
[39] http://www.tcd.ie/Physics/people/Cormac.McGuinness/Cowan/
[40] S. Fritzsche Computer Physics Communications, 183, 1525 (2012)
[41] F. A. Parpia, C. F. Fischer, I. P. Grant, Comput. Phys. Commun, 94, 249 (1996)
[42] P. Jönsson, X. He, C. Froese Fischer, I. P. Grant, Comput. Phys. Commun. 177, 597 (2007)
[43] S. Fritzsche et al, J. Phys. B 38 (2005) S707; S. Fritzsche et al, Phys. Rev. A 78 (2008) 032703; S. Fritzsche et al, Phys. Rev. Lett., 103 (2009) 113001
[44] M: Sewtz et al., Phys. Rev. Lett., 90 (2993) 163002
[45] C. Z. Dong et al, MNRAS, 369 (2006) 1735
[46] J. Bieron et al., J: Phys. B, 37 (2004) L305; J. Bieron et al., Phys. Rev. A, 80 (2009) 012530
[47] Busquet M., Klapisch M., Bar-Shalom A., J. Quant. Spectr. Rad. Transfer 71, 225 (2001)
[48] Busquet M., A.Bar-Shalom, Klapisch M., Oreg J., J.Phys. IV France 133, 973 (2006)
[49] M. F. Gu, Can. J. Phys., 86 (2008) 675
[50] http://sprg.ssl.berkeley.edu/~mfgu/fac/
[51] X. Gonze et al, Comput. Phys. Comm. 180 (2009) 2582
[52] http://www.abinit.org/
[53] J. MacFarlane, Comput. Phys. Comm. 56 (1989) 259
[54] T.A. Helmes and G. A. Moses, Comput. Phys. Comm. 183 (2012) 2629
[55] C. Bhattacharya et al., J. Appl. Phys., 102 (2007) 064915
[56] R. M. More, Adv. At. Mol. Phys., 21 (1985) 305
[57] G. Faussurier, C. Blancard and P. Renaudin, HEDP, 4 (2008) 114
[58] M. Busquet et al., HEDP, 5 (2009) 270
[59] H. A. Scott, Journal of Quantitative Spectroscopy and Radiative Transfer, 71, 689 (2001)
[60] H. A. Scott and S. B. Hansen, High Energy Density Physics, 6, 39 (2010)
[61] http://www.llnl.gov/def_sci/cretin
[62] Scofield J H 1972 1974 At. Data Nucl Data Tables 14 121
[63] J. J. MacFarlane et al, High Energy Density Phys. 3 (2007) 181
[64] http://www.prism-cs.com/index.htm
[65] J. P. Christiansen et al, Comput. Phys. Comm. 7 (1974) 271
[66] R. Ramis, R. Schmalz and J. Meyer-Ter-Vehn, Comput. Phys. Comm. 49 (1988) 475
[67] http://138.4.113.100/multi/index.html
[68] R. Ramis, J. Meyer-Ter-Vehn and J. Ramirez, Comput. Phys. Comm. 180 (2009) 977
[69] S. V. Zakharov, V. G. Novikov and P. Choi, "Z* code for DPP and LPP source modelling" P.223 in "EUV sources for Lithography", Ed. V. Bakshi, SPIE Press (2005); S. V. Zakharov, P. Choi, A. Y. Krukovskiy, V. G. Novikov, V. S. Zakharov, EUV Source Workshop Vancouver BC, Cannada, May 25, 2006
[70] F. Ogando and P. Velarde, J. Quant. Spectrosc. Radiat. Transf. 71, 541 (2001).
[71] G. J. Pert, J. Fluid Mech., 131 (1983) 401
[72] D. Bauer and P. Koval, Comput. Phys. Comm., 174 (2006) 396
[73] http://www.physik.uni-rostock.de/physik-forschung/arbeitsgruppen/qtmps/qprop/
[74] W. Kohn, L. J. Sham, Phys. Rev. 140 (1965) A1133
[75] R. Lichters et al, Phys. Plasmas 3(9), 3425 (1996), A. Kemp, R. Pfund and J. Meyer-Ter-Vehn, Phys. Plasmas 11 (12), 5648 (2004)

[76] http://lichters.net/download.html
[77] L.D. Landau, E.M. Lifshitz Quantum Mechanics Sec. Ed. Pergamon, Oxford (1965), p. 491
[78] C. S. Brady and T. D. Arber Plasma Physics and Controlled Fusion, 53, 015001 (2011)
[79] http://ccpforge.cse.rl.ac.uk/gf/project/epoch/
[80] C. Buth and R. Santra, Phys. Rev. A, 75 (2007) 033412, Christian Buth and Robin Santra, "FELLA (Free Electron Laser Atomic, Molecular, and Optical Physics Program Package), Version 1.3.0, Argonne National Laboratory, Argonne, Illinois, USA, with contributions by Mark Baertschy, Kevin Christ, Chris H. Greene, Hans-Dieter Meyer, and Thomas Sommerfeld (2007)
[81] https://wiki-ext.aps.anl.gov/amo/index.php/Main_Page
[82] D. L. Windt, Computers in Physics, 12, 360-370 (1998))
[83] http://www.rxollc.com/idl/
[84] http://www.radiantzemax.com/
[85] F. Schäfers, "The BESSY Raytrace Program RAY" in "Modern developments in X-ray and Neutron Optics", Ed. by A. Erko, M. Idir, T. Krist and A. Michette, Springer series in Optical Sciences, vol. 137 (2007)
[86] https://www.helmholtz-berlin.de/forschung/grossgeraete/nanometeroptik/methods/software_en.html
[87] H. O. Moser et al, in 'Developments in X-Ray Tomography VI', Proceedings of SPIE Vol. 7078, 707814, (2008)
[88] http://www.ts-imaging.net/WebHelp/X-TRACT/X-TRACT.htm
[89] http://www.ts-imaging.net/Services/

MODELLING OF PLASMA-BASED SEEDED SOFT X-RAY LASERS

E. Oliva, T. T. Thuy Le and P. Zeitoun

Laboratoire d'Optique Appliquée, ENSTA ParisTech, Ecole Polytechnique ParisTech, CNRS, Chemin de la Hunière, 91761, Palaiseau, France

1 INTRODUCTION

The development of bright sources of coherent soft X-rays is of major current interest. Free-electron lasers (FELs), seeded plasma-based soft X-ray lasers and high harmonic generation (HHG) sources are being applied in diverse fields such as biology[1] and physics.[2] However, only FELs provide the energy (~10 μJ) and the ultra-high intensity (>10^{16} W / cm^2) needed for breakthrough experiments such as single-shot imaging of samples with characteristic evolution times in the femtosecond range.[3] On the other hand, plasma-based soft X-ray lasers have demonstrated the highest energy per pulse (10 mJ),[4] but the spatial coherence is weak and the pulse durations are hundreds of picoseconds; these two drawbacks prevent such sources from achieving the ultra-high intensity needed for the most demanding applications.

The technique of seeding high order harmonics in a plasma amplifier overcomes these problems, as the amplified high harmonics conserve the good wavefront and spatial coherence of a short pulse while extracting the energy stored in the amplifier.[5–11] When seeding in gas amplifiers the resulting beam is fully polarized and has, as expected, a high degree of coherence[6] and a diffraction-limited wavefront. However, the pulse duration is still too long for applications (around 5 ps) and the energy is still not sufficient (about 1 μJ). The next logical step is to seed denser plasmas, created from solid targets. As the density is higher, the amplifier can store more energy and the output pulse duration should decrease due to collisional line broadening.[12] Nevertheless, the energies obtained in experiments are less than 100 nJ and duration is still of the order of picoseconds.[11]

In order to explain these results and design an amplifier to deliver several millijoules in hundreds of femtoseconds, a thorough knowledge of the creation and evolution of the plasma amplifier and the propagation of the seed through the plasma is needed. In this chapter, the codes used to understand the processes involved on the amplification of coherent X-ray radiation in plasmas will be described along with the results obtained, opening the way towards ultra-intense (~10 mJ, ~200 fs) fully coherent soft X-ray lasers.

2 SOFTWARE

Modelling the full setup of a multi-stage, plasma-based seeded soft X-ray laser is a huge enterprise as it involves several physical processes, including laser absorption and propagation in plasmas, plasma hydrodynamics, atomic physics and electromagnetism. These have different spatial and temporal characteristic scales, from some femtoseconds for the amplification of high harmonics in the plasma to several nanoseconds during the creation and evolution of the plasma amplifier – about six orders of magnitude. Solving the complete multidimensional problem would require complicated software (in terms of computational science and physics) running in large parallel computers. As there are many different parameters which play a crucial role in the design of these experiments, it is completely impractical to use such an approach. Thus, some simplification is needed to reduce the complexity and computational cost of the tools.

The first simplification consists of dividing the problem into different physical regimes, which can then be solved separately instead of in a coupled way. This means that each problem is treated with optimal techniques and approximations which reduce the computational cost and enhance the accuracy of the results. In addition to this, as there are fewer free parameters, it is easy to optimize several parts of the system separately, such as the laser parameters to create the amplifier and the high harmonic energy and duration. In the case treated here, the creation and evolution of the amplifier (plasma hydrodynamics) is decoupled from the other processes. Some parameters of interest which depend on the atomic physics can be calculated by post-processing the hydrodynamic data and effectively coupling with the high harmonic electromagnetic field propagation through the amplifier in order to model the amplification of the seeded harmonics and the evolution of atomic populations in time via the Maxwell-Bloch equations.[13]

3 THE ARWEN CODE

The creation of a plasma from a solid target and its evolution in time is modelled using the two dimensional hydrodynamic code ARWEN, which also takes into account electron thermal conduction and radiation transport.[14] It has been developed and is maintained by the Instituto de Fusión Nuclear of the Universidad Politécnica de Madrid, Spain. It has been applied in several different fields, such as inertial confinement fusion,[15] laboratory astrophysics[16] and plasma-based seeded soft X-ray lasers.[17,18,19] ARWEN solves the radiation hydrodynamics equations (1)–(8) with thermal conduction

$$\frac{\partial \rho}{\partial t} + \nabla \rho \, \vec{\boldsymbol{u}} = 0 \tag{1}$$

$$\frac{\partial \rho \vec{u}}{\partial t} + \nabla \rho \, \vec{\boldsymbol{u}} \, \vec{\boldsymbol{u}} = -\nabla\left(\overrightarrow{P_m} + \overrightarrow{P_r}\right) \tag{2}$$

$$\frac{\partial \rho E_m}{\partial t} + \nabla\left[\rho E_m \, \vec{\boldsymbol{u}} + \left(\overrightarrow{P_m} + \overrightarrow{P_r}\right)\vec{u}\right] = S_E + \nabla\overrightarrow{q_c} + \nabla\overrightarrow{q_r} \tag{3}$$

$$\Omega \nabla \vec{\mathrm{I}} + \vec{\kappa}\vec{\mathrm{I}} = \varepsilon \tag{4}$$

$$\nabla\overrightarrow{\mathrm{q_c}} = -\nabla\left(\overrightarrow{\mathrm{k_e}}\nabla \mathrm{T}\right) \tag{5}$$

$$\nabla\overrightarrow{q_r} = \int \left(\vec{\kappa}\vec{I} - \varepsilon\right) d\upsilon \tag{6}$$

$$E_r = \frac{1}{c}\int I \, d\Omega \, d\upsilon \tag{7}$$

$$P_r = \frac{1}{3} E_r \tag{8}$$

In these equations, ρ is the density, $\mathbf{u}$ is the velocity vector, $\mathbf{P}_m$ and $\mathbf{P}_r$ are the matter and radiation pressure tensors, E_m is the energy of the matter (kinetic and internal energy of the plasma), S_E is the laser energy source i.e. the laser energy absorbed by the plasma, $\mathbf{q}_c$ and $\mathbf{q}_r$ are the heat fluxes due to conduction and radiation, c is the speed of light, $\mathbf{I}$ is the radiation intensity, Ω is the solid angle in which radiation propagates, $\boldsymbol{\kappa}$ and ε are the opacity and the emissivity of the plasma, $\mathbf{k}_e$ is the thermal conductivity, v is the frequency of the radiation and E_r is the energy of the radiation field.

The numerical solutions of equations (1)–(8) require a range of different approaches, including integral equations and hyperbolic and elliptical partial derivative equations (PDEs). Thus it is necessary to treat each subset of the equations with a solver adapted to that particular problem.

The compressible Navier-Stokes equations (1–3), including radiation pressure and radiation heat transfer, are solved with an Eulerian scheme using a high-order Godunov method with an approximate Riemann solver.[20] The flux-limited thermal electron conduction equation (5) and the radiation transport equations (4,6) are treated with multi-grid[21] and Sn (discrete ordinates method, where the solid angle is discretized into several regions) multi-group methods[22,23] respectively. Matrix-free solvers for thermal conduction are available in the new version of the code.

As usual when working with compressible Navier-Stokes equations, a closing relation, i.e., an equation of state (EOS), is needed to solve the system. The ARWEN code does not compute the EOS each timestep for each mesh cell as it would be too expensive computationally. Instead, the EOS data is created once and written into a table. The ARWEN code reads the appropriate value from the table and, if necessary, interpolates it, which is faster than computing the EOS itself.

The EOS data are obtained from the quotidian equation of state (QEOS),[24] and the multipliers are adjusted to fit experimental data as Hugoniot curves. Opacities are computed with the JIMENA[25] and BiGBART codes, also developed at the Instituto de Fusión Nuclear.

Compressible fluid-like media with high energy density (such as laser produced plasmas) can develop structures including shockwaves and hydrodynamic instabilities which, to be resolved properly and reduce the numerical errors, need a very fine mesh in the modelling. Nevertheless, these structures appear only in a small part of the computational domain, most of the flow being regular. The majority of the flow is therefore well resolved using a coarse grid, with some small regions needing a finer grid. As using the finest grid in the whole domain will result in a waste of computational time, and so special meshing techniques must be used. The ARWEN code and all its packages are based on the adaptive mesh refinement (AMR) technique.[26,27] This consists of putting patches of finer grids only in the regions where they are needed, producing a uniform numerical error and saving computational time. The structure of levels and grids is created and controlled by the C++ library BoxLib.

4 ATOMIC PHYSICS

As explained above, the atomic physics related to the creation of gain inside the amplifier are decoupled from the hydrodynamic calculations (a newer version of the ARWEN code will couple temporal ionization dynamics and thus the gain calculation with the standard hydrodynamic model). Hence parameters of interest such as gain and saturation fluence must be calculated by post-processing the hydrodynamic data given by ARWEN. To simplify the calculations, a simple three-level atomic model was used, as shown in figure 1.

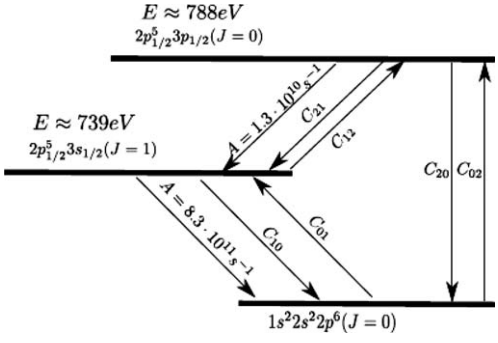

Figure 1 *Simplified Grotrian scheme and transitions of neon-like iron used in the post-processing calculations, using published data.*[28,29]

The lasing transition is $2p^5_{1/2}3p_{1/2}\ J=0 \rightarrow 2p^5_{1/2}3s_{1/2}\ J=1$ in neon-like iron (Fe^{16+}) at $\lambda = 25.5$ nm. The fundamental level (0) is assumed to be much more populated than the lower (1) and upper (2) levels and so its population can be assumed to be constant. To assure the creation of a population inversion between levels 1 and 2, the radiative transition between the level 2 and the fundamental level must be forbidden. In addition to this, level 1 must decay quickly to the fundamental level. With these conditions, electron collisional excitation can create the population inversion.[30,31,32]

In this model, the populations of levels 1 and 2 are calculated by solving the stationary rate equations

$$\frac{\mathrm{d}N_i}{\mathrm{d}t} = \sum_j C_{ij} n_\mathrm{e} N_j + \sum_j A_{ij} N_i, \tag{9}$$

$$\frac{\mathrm{d}N_i}{\mathrm{d}t} = 0, \tag{10}$$

where N_i is the population of level i, n_e is the electron density, A_{ij} is the Einstein spontaneous emission coefficient of the transition and the C_{ij} are the collisional (de)excitation rates between levels i and j. The electron collisional rates are computed using Van Regemorter's formula,[33] equation (11) using the electron density and temperature given by the ARWEN code and assuming a Maxwellian distribution of electron speeds. The detailed balance principle allows the inverse process rate to be computed, equation (12),

$$C_{ij} \approx 1.6\times10^{-5}\frac{f_{ij}\langle g\rangle}{\Delta E_{ij}\sqrt{kT_{\mathrm{e}}}}e^{-\Delta E_{ij}/k_{\mathrm{B}}T_{\mathrm{e}}}, \tag{11}$$

$$C_{ji} \approx \frac{\gamma_i}{\gamma_j}C_{ij}e^{\Delta E_{ij}/k_{\mathrm{B}}T_{\mathrm{e}}}, \tag{12}$$

where f_{ij} is the oscillator strength, <g> is the Gaunt factor 0.2 in this case), k_{B} is the Boltzmann constant, T_{e} is the electron temperature, ΔE_{ij} is the energy difference between the levels and γ^i is the degeneracy of level i.

Once the populations of the levels involved in the transition have been determined, the small signal gain, equation (13), and the saturation fluence, equation (14), both at the line centre, can be calculated

$$g_0^{\mathrm{ss}}\left(\nu=\nu_0\right)=\left(N_2-\frac{\gamma_2}{\gamma_1}N_1\right)\sigma_{\mathrm{stim}}\left(\nu=\nu_0\right), \tag{13}$$

$$F_{\mathrm{sat}}\left(\nu=\nu_0\right)=\frac{h\nu_0}{\sigma_{\mathrm{stim}}\left(\nu=\nu_0\right)}, \tag{14}$$

where ν_0 is the frequency at the line centre, σ_{stim} is the stimulated emission cross-section and h is the Planck constant. In order to easily compute the cross-section, it is necessary to make a final assumption about the line profile throughout the plasma amplifier. In this case, only Doppler broadening is taken into account and the resulting formulae are

$$\sigma_{\mathrm{stim}}\left(\nu\right)=\Phi\left(\nu\right)\frac{\lambda^2}{8\pi}A_{21}, \tag{15}$$

$$\Phi_{\mathrm{D}}\left(0\right)=\lambda\left(\frac{m_{\mathrm{i}}}{2\pi k_{\mathrm{B}}T_{\mathrm{i}}}\right)^{1/2}, \tag{16}$$

where $\Phi(\nu)$ is the Doppler spectral profile of the line, $\Phi_{\mathrm{D}}(0)$ is the value of the Doppler spectral profile at the line centre, m_{i} is the ion mass and T_{i} is the ion temperature. Using this analysis, it is possible to estimate the amplification of the intensity and energy as a function of length in the plasma by solving the ordinary differential equation

$$\frac{\mathrm{d}E}{\mathrm{d}x}=g_0I=\frac{g_0^{\mathrm{ss}}}{1+E/E_{\mathrm{sat}}}E \tag{17}$$

where E is the energy, g_0 is the gain and E_{sat} is the saturation energy (the product of F_{sat} and the area). The solution of this equation for different values of small signal gain and saturation energy is shown in figure 2, demonstrating the characteristic shape of typical amplification curves. In the first few hundred micrometres there is no apparent amplification. In this part of the amplifier, the broad harmonic linewidth decreases until it fits the amplifier bandwidth, at which point exponential amplification begins – the steep parts of the curves. In this regime, the beam is strongly amplified until it reaches the saturation energy, after which the amplified beam is intense enough to depopulate the upper level of the transition appreciably, destroying population inversion and thus reducing amplification. This saturation regime starts, for the situation reported in figure 2, when the beam has passed through 1-2 mm of plasma, when the gain-length product has a characteristic value of around 18.

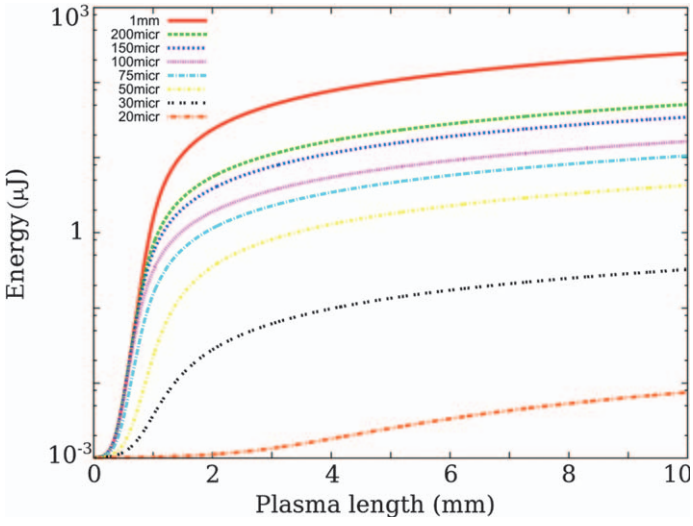

Figure 2 *Energy amplification as a function of plasma length for different plasma widths..*

4.1 Propagation Through Inhomogeneous Media

Laser created plasmas are strongly inhomogeneous media with large electron density gradients which induce refractive index gradients, causing the seeded beam to deviate from a straight trajectory. This results in the seeded beam to exit the gain zone, inhibiting amplification. The understanding of this effect is crucial in order to effectively amplify the beam.

Since seeded soft X-ray lasers are directional (namely the propagation direction through the plasma) it is possible to apply ray-tracing techniques to model the refraction (and amplification) of the seeded beam. As an example, figure 3 shows the results of post-processing of the ARWEN data given by three-dimenional ray-tracing code SHADOX (developed by the Laboratoire d'Optique Appliquée, France, and the Instituto Superior Tecnico, Portugal).

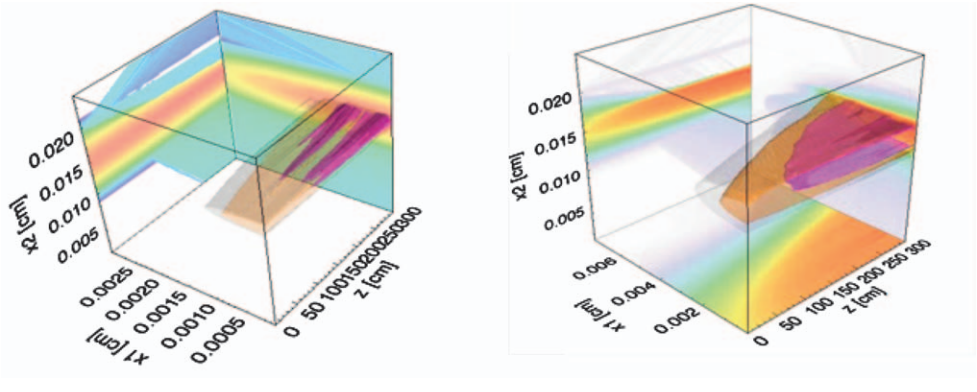

Figure 3 *Amplification and spatial shape of the seeded beam through (left) an inhomogeneous target and (right) a more homogeneous target. The simulations were done using the 3D ray-tracing code SHADOX.*

Figure 3 shows the evolution of the beam through the plasma for different electron density gradients. The gradient is steeper in the figure on the left, resulting in filamentation and degradation of the beam. The beam in the figure on the right is much more homogeneous, as the electron density varies slowly and thus refraction effects are less important.

4.2 Maxwell-Bloch simulation of the amplification of radiation.

As explained in the preceding sections, post-processing the hydrodynamic data given by ARWEN gives valuable information on how to seed correctly in order to minimize refraction effects and about the energy and spatial shape of the output beam. However, it is not possible to obtain information about the temporal profile of the output beam, although estimating the line broadening can give some limiting values about the duration of the pulse[12] but not a detailed picture of the temporal energy distribution. In addition the dynamic populations and dynamic effects induced in the beam (such as Rabi oscillations) cannot be studied with such post-processing since the equations are solved for the steady state.

In order to take these temporal effects into account, it is necessary to couple the atomic physics results with the electromagnetic field and solve the equations both spatially and temporally. Because of the different timescales involved in the processes, from tens of femtoseconds (high harmonic pulse duration) to picoseconds (plasma response), Maxwell-Bloch type equations must be used.

The Maxwell-Bloch equations can be deduced from the Maxwell wave equation for electric fields propagating through plasmas,

$$\Delta\vec{E} - \frac{1}{c^2}\frac{\partial^2\vec{E}}{\partial t^2} - \frac{\omega_p^2}{c^2}\vec{E} = \mu_0\frac{\partial^2\vec{P}}{\partial t^2} \tag{18}$$

where ω_p is the plasma frequency, μ_0 is the vacuum permeability and **P** is the polarization density of the medium. Assuming a monochromatic field of frequency ω_0, and in the slowly varying envelope approximation (neglecting second derivatives of the electric field and first derivatives of the polarization), equation (18) can be rewritten, for the direction of propagation, z, as

$$\frac{2i\omega_0}{c^2}\left(\frac{\partial E}{\partial t} + c\frac{\partial E}{\partial z}\right) = -\frac{\omega_0^2}{c^2}\left(-\frac{\omega_p^2}{\omega_0^2}E + \mu_0 c^2 P\right). \tag{19}$$

Changing from the laboratory frame to the photon frame reduces this partial differential equation to an ordinary differential equation, which is much easier to solve. The change of variable is $\tau = t - z/c$ where τ is the reduced time. Defining $\xi = c\tau$ gives

$$\frac{\partial E}{\partial \xi} = \frac{i\omega_0}{2c}\left[\mu_0 c^2 P - \left(\frac{\omega_p}{\omega_0}\right)^2 E\right]. \tag{20}$$

The amplification (first term in square brackets) and damping (second term) of the electric field through the plasma is described by equation (20). As usual, a constitutive relation (a relation between two physical quantities, specific of a material, that approximates its response to external fields) which relates polarization and material properties is needed. In this case, polarization is given by

$P = \mathrm{Tr}(\boldsymbol{\rho} d)$ where $\boldsymbol{\rho}$ is the density operator, d the atomic electric dipole and Tr denotes the trace of the matrix. The Zeeman coherences can be neglected and the resulting equation for polarization is[34]

$$\frac{\partial P}{\partial \tau} = \Gamma - \gamma P - \frac{\mathrm{i} z_{21}^2}{\hbar} E\left(N_2 - N_1\right) \tag{21}$$

where a source term Γ has been added to model the spontaneous emission. This term has a vanishing correlation time and it is normalized to obtain (via the Wiener-Khinchine theorem) the correct Lorentzian line width.[35] The depolarization term γ is given approximately by the electron-ion collision frequency. Z_{21} is the dipole matrix element.

Finally, the populations N_1, N_2 appearing in equation (21) are computed using standard rate equations, explained in section 4, but taking into account the temporal dependence and adding a term coupling the populations and the electric field

$$\frac{\partial N_2}{\partial t} = \sum_k C_{k2} N_k + \frac{\mathrm{Im}\left(E^* P\right)}{2\hbar} \tag{22}$$

$$\frac{\partial N_1}{\partial t} = \sum_k C_{k1} N_k - \frac{\mathrm{Im}\left(E^* P\right)}{2\hbar}. \tag{23}$$

The Einstein A coefficients are included in the C coefficients. This set of equations (20)-(23) are the so-called Maxwell-Bloch equations. When solved properly (using high order Runge-Kutta methods for example), the amplification of the seeded pulse and the evolution of the temporal and spatial shapes of the pulse are obtained, as shown in figure 4.

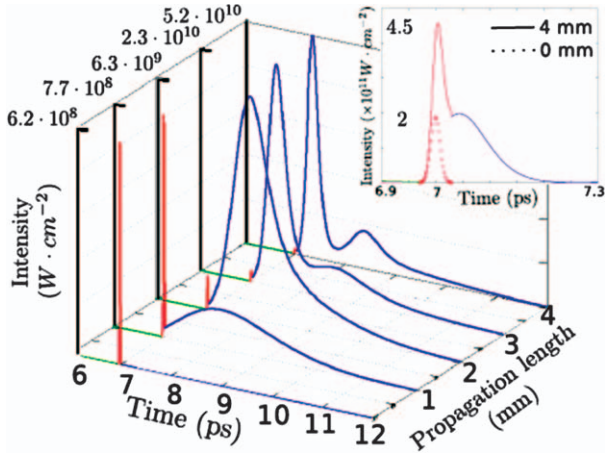

Figure 4 *Temporal shape of the seeded high harmonic through the plasma amplifier. The typical structure of harmonic and wake (representing Rabi oscillations and coherent decay) is observed.*[36–39]

5 VISUALIZATION

The data given by the programs described above consists of arrays of numbers. Although these numerical data are needed to make quantitative physical predictions, in order to describe the temporal evolution of the system and gain a deep knowledge of the problem some visualization tool is necessary. Images and/or videos are valuable tools since spatial structures, such as jets or gradients, and their evolution in time can be easily recognized.

Although most programs have their own tools to check the simulations and to study the physics, sometimes it is better to use more powerful visualization. This adds one more step to the analysis as the output data must be written in a format compatible with the visualization tool. This can be done by modifying the program itself (changing the output subroutines) or by post-processing the data. The solution adopted depends on each particular case — how difficult it is to modify the source code, how many simulations are already done, and so on.

As an example, figure 5 shows a 3D image of the electron density and gain of a plasma simulated using ARWEN; the image was made using VisIt.[40] As explained, the 2D data given by ARWEN was post-processed to obtain the gain. Then, both sets of data were rewritten in the format required by VisIt, making it possible to create 3D images, combine different sets of data (in this case gain and electron density) and find the best conditions (angle, illumination, transparency, etc.) to best understand the physics involved.

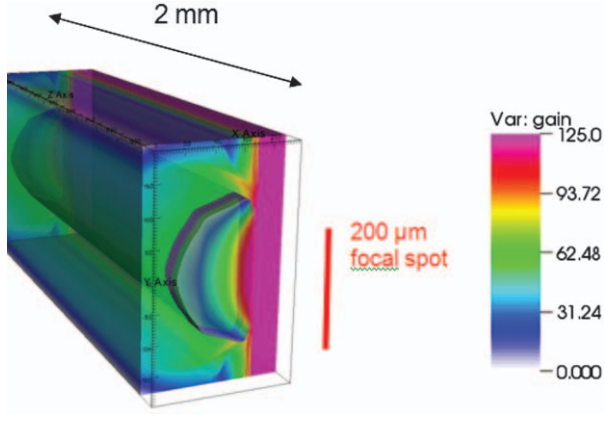

Figure 5 *3D image of electron density and gain of a plasma simulated with ARWEN. The gain zone is shown embedded into the plasma. Some structures such as lateral jets can be seen. The figure was created using VisIt.*[40]

6 CONCLUSIONS

In this chapter we have reviewed the modelization of seeded soft X-ray lasers using plasma amplifiers from solid. Since these sources present different temporal and spatial scales from nanoseconds (plasma characteristic time), picoseconds (atomic system) and femtoseconds (HOH electric field envelope), specific multiscale tools are needed. The creation and evolution of the plasma amplifier is studied with a 2D hydrodynamic code, optimized for this kind of problem. Atomic parameters, as gain and saturation fluence, are

obtained postprocessing hydrodynamic data. Then, amplification is studied in different ways : a 3D ray-tracing code is used to study the role of refraction and focusing in the amplification process, whereas a Maxwell-Bloch code is used to model the temporal evolution of the seeded radiation and its coupling with the atomic system. Powerful visualization tools are also used to properly display the 3D properties of the system. The results obtained with these computational tools provide an invaluable aid to comprehend experimental results and design and optimize new schemes, by identifying the key parameters of the experiments.

References

1 R.E. Burge, M.T. Browne, P. Charalambous, G.E. Slark and P.J. Smith, *Opt. Lett.*, 1993, **18**, 661.
2 J. Itatani, J. Levesque, D. Zeidler, H. Niikura, H. Pépin, J.C. Kieffer, P.B. Corkum and D.M. Villeneuve, *Nature*, 2004, **432**, 867.
3 H.N. Chapman, *Nature Mater*., 2009, **8**, 299.
4 B. Rus, T. Mocek, A.R. Präg, M. Kozlová, G. Jamelot, A. Carillon, D. Ros, D. Joyeux, and D. Phalippou, *Phys. Rev.*, 2002, **A66**, 063806.
5 T. Ditmire, M.H.R. Hutchinson, M.H. Key, C.L.S. Lewis, A. MacPhee, I. Mercer, D. Neely, M.D. Perry, R.A. Smith, J.S. Wark and M. Zepf, *Phys. Rev.*, 1995, **A51**, R4337.
6 P. Zeitoun, G. Faivre, S. Sebban, T. Mocek, A. Hallou, M. Fajardo, D. Aubert, P. Balcou, F. Burgy, D. Douillet, S. Kazamias, G. de Lachèze-Muriel, T. Lefrou, S. le Pape, P. Mercère, H. Merdji, A.S. Morlens, J.P. Rousseau and C. Valentin, *Natur*e, 2004, **431**, 426.
7 Y. Wang, E. Granados, M.A. Larotonda, M. Berrill, B.M. Luther, D. Patel, C.S. Menoni and J.J. Rocca, *Phys. Rev. Lett.*, 2006, **97**, 123901.
8 N. Hasegawa, T. Kawachi, A. Sasaki, M. Kishimoto, K. Sukegawa, M. Tanaka, R.Z. Tai, Y. Ochi, M. Nishikino, K. Nagashima and Y. Kato, *Phys. Rev.*, 2007, **A76**, 043805.
9 Y. Wang, E. Granados, F. Pedaci, D. Alessi, B. M. Luther, M. Berrill and J.J. Rocca, *Nature Photonics*, 2008, **2**, 94.
10 F. Pedaci, Y. Wang, M. Berrill, B. Luther, E. Granados and J.J. Rocca, *Opt. Lett.*, 2008, **33**, 491.
11 Y. Wang, M. Berrill, F. Pedaci, M.M. Shakya, S. Gilbertson, Z. Chang, E. Granados, B.M. Luther, M.A. Larotonda and J.J. Rocca, *Phys. Rev.*, 2009, **A79**, 023810.
12 D.S. Whittaker, M. Fajardo, P. Zeitoun, J. Gautier, E. Oliva, S. Sebban and P. Velarde, *Phys. Rev.*, 2010, **A81**, 043836.
13 Y. Castin and K. Mølmer, *Phys. Rev.*, 1995, **A51**, R3426.
14 F. Ogando and P. Velarde, *J. Quant. Spectrosc. Radiat. Transf.*, 2001, **71**, 541.
15 P. Velarde, F. Ogando, S. Eliezer, J. Martínez-Val, J. Perlado and M. Murakami, *Laser Part. Beams*, 2005, **23**, 43.
16 P. Velarde, D. García-Senz, E. Bravo, F. Ogando A.R. Relaño, C. García and E. Oliva, *Phys. Plasmas*, 2006, **13**, 092901.
17 K. Cassou, P. Zeitoun, P. Velarde, F. Roy, F. Ogando, M. Fajardo, G. Faivre and D. Ros, *Phys. Rev.*, 2006, **A74**, 045802.
18 E. Oliva, P. Zeitoun, S. Sebban, M. Fajardo, P. Velarde, K. Cassou and D. Ros, *Opt. Lett.*, 2009, **34**, 2640.
19 E. Oliva, P. Zeitoun, P. Velarde, M. Fajardo, K. Cassou, D. Ros, S. Sebban, D. Portillo and S. le Pape, *Phys. Rev. E*, 2010, **82**, 056408.
20 P. Colella and H.M. Glaz, *J. Comput. Phys.*, 1985, **59**, 264.

21 S.F. McCormick and R.E. Ewing, *Multigrid Methods*, 1987, (Philadelphia: SIAM).
22 S. Chandrasekhar, *Radiative Transfer*, 1960, (Dover Publications: New York).
23 K.D. Lathrop, *Nucl. Sci. Eng*., 24, 381 1966.
24 R.M. More, K.H. Warren, D.A. Young and G.B. Zimmerman, *Phys. Fluids*, 1988, **31**, 3059.
25 E. Minguez and R. Falquina, *Laser Part. Beams*, 1992, **10**, 651.
26 M.J. Berger and P. Colella, *J. Comput. Phys.*, 1989, **82**, 64.
27 C.A. Rendleman, V.E. Beckner, M. Lijewski, W. Crutchfield and J.B. Bell, *Comput. Visualization Sci.*, 2000, B, 147.
28 T. Shirai, Y. Funatake, K. Mori, J. Sugar, W. L. Wiese, and Y. Nakai, J. Phys. Chem. Ref. Data 19, 127 1990.
29 J.A. Koch, B.J. MacGowan, L.B. Da Silva, D.L. Matthews, J.H. Underwood, P.J. Batson, R.W. Lee, R.A. London and S. Mrowka, *Phys. Rev.*, 1994, **A50**, 1877.
30 B.L. Whitten, A.U. Hazi, M.H. Chen and P.L. Hagelstein, *Phys. Rev.*, 1986, **A33**, 2171.
31 W.H. Goldstein, B.L. Whitten, A.U. Hazi and M.H. Chen, *Phys. Rev.*, 1987, **A36**, 3607.
32 P.V. Nickles, V.N. Shlyaptsev, M. Kalachnikov, M. Schnurer, I. Will and W. Sandner, *Phys. Rev. Lett.*, 1997, **78**, 2748.
33 H.V. Regemorter, *Astrophys. J.*, 1962, **136**, 906.
34 A. Sureau and P.B. Holden, *Phys. Rev.*, 1995, **A52**, 3110.
35 O. Larroche, D. Ros, A. Klisnick, A. Sureau, C. Möller and H. Guennou, *Phys. Rev.*, 2000, **A62**, 043815.
36 I.R. Al Miev, O. Larroche, D. Benredjem, J. Dubau, S. Kazamias, C. Möller and A. Klisnick, *Phys. Rev. Lett.*, 2007, **99**, 123902.
37 C.M. Kim, K.A. Janulewicz, H.T. Kim and J. Lee, *Phys. Rev.*, 2009, **A80**, 053811.
38 C.M. Kim, J. Lee and K.A. Janulewicz, *Phys. Rev. Lett.*, 2010, **104**, 053901.
39 E. Oliva, P. Zeitoun, M. Fajardo, G. Lambert, D. Ros, S. Sebban and P. Velarde, *Phys. Rev.* A, 84,013811 (2011).
40 https://wci.llnl.gov/codes/visit/

FIELD COHERENCE OF EUV SOURCES

Olivier Guilbaud

Laboratoire de Physique des Gaz et Plasma, Unité Mixte CNRS Université Paris-Sud, France

1 INTRODUCTION

As sources of electromagnetic radiation provide shorter wavelengths, optical instrumentation and techniques must keep pace. Such evolution take the form of extrapolation or adaptation of concepts well known at longer wavelengths; the ability to measure the wavefront properties of sources has the same importance in the extreme ultraviolet (EUV) range as in the visible and, for this reason, Hartmann and Shack-Hartmann sensors have been adapted to very short wavelengths.[1] For example, they have been used to characterize high order harmonic beams and synchrotron beamlines, and are being tested for use at advanced X-ray sources such as the Linac Coherent Light Source (LCLS) X-ray free electron laser (XFEL). However, the characteristics of short wavelength radiation also require the development of new techniques in order to measure novel properties of the source. An example is the RABBITT (reconstruction of attosecond beating by interference of two photon transitions) technique[2] which was developed to measure the relative spectral phase of high order harmonics in the context of attosecond pulse train generation and uses IR-XUV photo-ionisation as a coherent nonlinear process from which the attosecond structure can be extracted. Adapting the general theory of coherence to shorter wavelengths is straightforward, and methods for measuring the coherence properties of the source are usually direct adaptations of classical techniques, namely wavefront and amplitude division interferometers. However, this does not mean there are no challenges to short wavelength coherence measurement and utilisation.

These challenges include

- Technical challenges. Interferometry requires optics with excellent flatness with respect to the wavelength, which becomes more demanding to achieve as the wavelength decreases. In addition, grazing or multilayer optics must be used to provide high reflectivities. A specific difficulty arises when considering amplitude division interferometers, since EUV beamsplitters will be needed.
- *Modelling challenges*. The diversity of short wavelength sources is such that they encompass all the classical approximations usually made in theoretical optics. Some sources can be considered as fully coherent (e.g., high order harmonics),

whereas EUV lines emitted by laser produced or discharge plasmas can be considered as spatially incoherent at the source and with a random temporally stationary field. It is more significant that many sources lie between these two limiting cases. The XFEL and transient soft X-ray lasers rely on (self) amplification of spontaneous emission, or (S)ASE, leading to partially coherent features and a breakdown of the stationary hypothesis.

Despite these difficulties, there are many potential applications of the coherent properties of short wavelength sources, including the following. First, because of the short wavelength, interferometric methods will provide high sensitivity on the evolution of surfaces.[3] EUV radiation can penetrate very dense plasmas and any shift in the interferometric pattern will provide information on the local refractive index and thus on the plasma electron density. Next, holography[4,5] and coherent diffraction at short wavelengths are powerful tools for producing time resolved images of nano-samples or macromolecules that are difficult to crystallize. Also, interference patterns produced by powerful sources can be used for permanent nano-patterning of surfaces or to generate a spatially modulated transient excitation of a sample (transient grating pump-probe methods).

The basics of coherence theory are well established[6] and so only a summary is given in the following section. Illustration related mainly to the development of high order harmonics and plasma based soft X-ray lasers will be given. The physics of such sources is detailed in other chapters of this book. The last parts of the present chapter provide a general framework of coherence properties applicable to all sources through the notion of spectral coherence.

2 SPATIAL AND TEMPORAL COHERENCE

2.1 Coherence Functions

Consider the complex representation of an optical field, $U(r,t)$, in the scalar approximation. From a theoretical point of view, the concept of coherence is related to correlations between different parts of the field. If the intensity, $|U(r,t)|^2$, is relatively smooth then phase correlations are the central aspect. The coherence function Γ is defined by:

$$\Gamma\left(r_1,r_2,t_1,t_2\right)=\left\langle U_1^*(r_1,t_1)U_2(r_2,t_2)\right\rangle, \tag{1}$$

where the bracket $\langle\rangle$ represents an ensemble average og all the field realizations. In the context of classical optical sources with pulse durations extremely long compared to the characteristic field evolution time (in this context, a random evolution), the field is assumed to be stationary and ergodic. The ensemble average is then equivalent to an average over an integration time long compared to this characteristic The stationarity of the field results in the time dependence of Γ depending only on the time difference $\tau = t_2 - t_1$,

$$\Gamma(r_1,r_2,t_1,t_2)=\Gamma(r_1,r_2,\tau). \tag{2}$$

Various useful functions related to experimentally measurable quantities can now be derived from Γ; for example, the average local intensity I is given by Γ when $\tau = 0$. In interferometry the fields U_1 and U_2 in the definition of Γ are related to an incoming field and interfere on a detector such as a CCD camera, producing fringes with visibility proportional to the modulus of Γ.

The spatial coherence function, defined by :

$$\Gamma(r_1, r_2) = \Gamma(r_1, r_2, \tau = 0), \tag{3}$$

can be used, for example, to predict the fringe visibility produced in a Young's slits experiment when the slits are located at r_1 and r_2. If r_1 is fixed (≡ 0), the modulus of the spatial coherence function globally decreases as $|r_2|$ increases. The width of the function $|\Gamma(0,r_2)|$ is called the spatial coherence length, Λ_T .Various definitions of the width exists, including width at half maximum, width at 1/e or RMS width.

The temporal coherence function, defined by putting $r_1 = r_2 = r$ is:

$$\Gamma(r, \tau) = \Gamma(r, r, \tau), \tag{4}$$

It allows, for example, the prediction of the evolution of fringe visibility in a Michelson experiment (as needed for measuring temporal coherence) when the path difference $\delta = c\tau$ is changed. The width of the function $|\Gamma(r,\tau)|$ is called the temporal coherence time, τ_c, which again is defined in a variety of ways. Since fringe visibility also depends on the intensity balance between the two interfering beams, a normalised coherence function, the degree of coherence, is introduced,

$$\gamma(r_1, r_2, \tau) = \frac{\Gamma(r_1, r_2, \tau)}{\left[I(r_1) I(r_2, \tau)\right]^{1/2}}. \tag{5}$$

The spectral density $S(r,\omega)$, where ω is the angular frequency, is defined as the average squared modulus of the Fourier transform of the field U. The stationarity of the field then leads to the Wiener-Khintchine theorem[7]

$$\Gamma(r, \tau) = \int S(r, \omega) \exp(-i\omega\tau) d\omega \tag{6}$$

From a practical point of view, measuring the temporal coherence function in terms of τ provides access to the average spectral profile of the source through a Fourier transform.

2.2 EUV and Soft X-ray Spatial Coherence Measurement

The spatial coherence function of a source can be reconstructed by illuminating a set of Young's slits with different separations. The evolution of the fringe visibility at the centre of the fringe field, as a function of the slit separation, directly reflects the evolution of the spatial coherence function across the beam. An example is shown in figure 1, where this procedure has been applied to EUV beams (λ=32,8nm) emitted by a high order harmonic generation source, an unseeded soft X-ray laser, and this soft X-ray laser seeded with the harmonic beam[8]. This method is simple and efficient but interpretation of the results must be done with care. The spatial coherence is probed at two points at both side of the optical

axis, and it has to be assumed that the temporal coherence length is large compared to the path difference involved in the interference process.

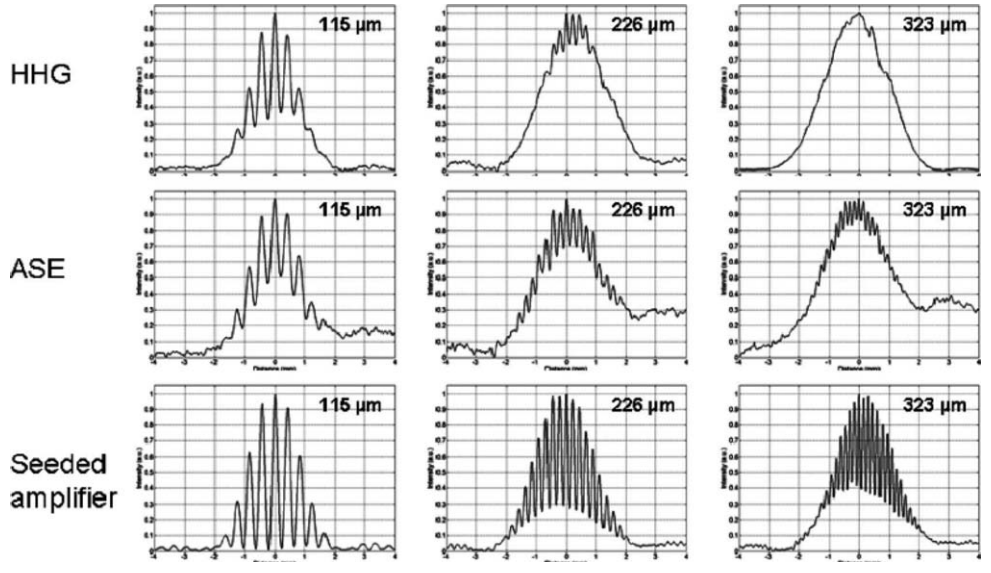

Figure 1 *Spatial coherence measurement with variable separation Young's slits (125,226 and 323 µm). Top: high order harmonics beam. Middle: plasma-based soft X-ray laser. Bottom: plasma-based soft X-ray laser seeded with harmonics.*[8]

2.3 EUV and Soft X-ray Temporal Coherence Measurement

A range of Michelson-like interferometric systems have been developed for the EUV and soft X-ray range. The instrument presented in figure 2 is a wavefront division interferometer where a Fresnel bimirror splits the incoming beam into two parts. The small angle between the mirrors leads to an overlap of the two secondary beams, and a detector placed in this overlapping region will record fringes. The system is designed to work at a small grazing angle α to obtain high reflectivity (α = 6°). The insert in figure 2 gives more details on the mirror shape; the dihedron geometry allows the introduction of a path difference between the beams by moving vertically one of the mirrors by an amount *z*. This operation does not change the spatial superposition of the beams, and thus any observed fringe visibility decrease will be associated to a temporal coherence loss and not to an uncontrolled spatial coherence loss. For this wavefront division interferometer, to obtain high fringe visibility the spatial coherence length has to be higher than the width of the interference field. If the source is spatially incoherent, the interferometer has to be placed far from it.

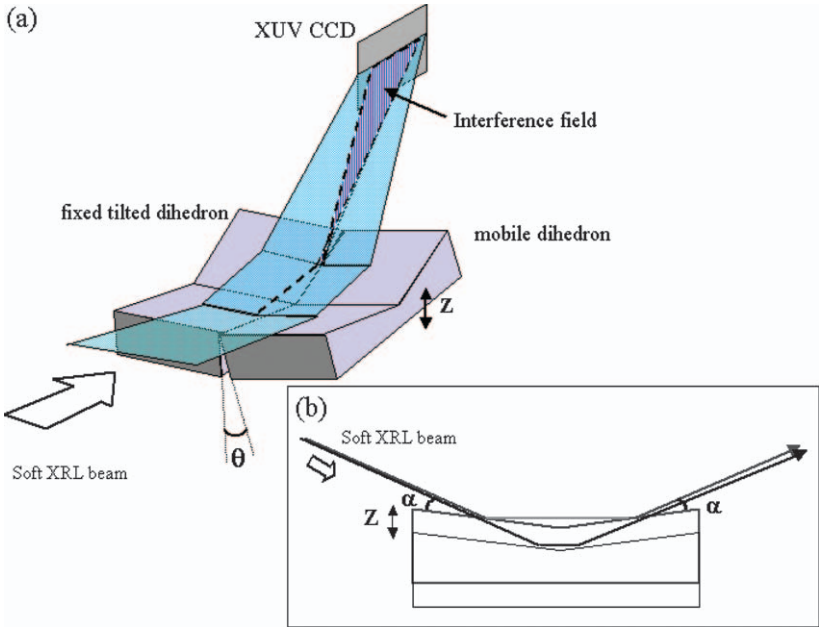

Figure 2 *Variable path difference interferometer based on the wavefront division principle. The insert shows the geometry of the fixed and mobile dihedra that enable a change in path difference without changing the overlap conditions of the interfering beams.*

3 COHERENCE PROPERTIES OF HIGH ORDER HARMONICS

3.1 Spatial, Temporal and Phase Coherence

The high order harmonics of an intense infrared laser beam inherit most of its coherence properties; the spatial coherence length covers the beam dimension of a single harmonic. Wavefront division interferometers are then particularly suitable and make interferometry experiments with this type of source more straightforward. A simple procedure can be used to measure the spatial coherence length of the harmonic beam after spectral selection. The contrast of the interference fringes produced in a classical Young's double slit experiment is measured as a function of slit separation as shown in figure 1.

The coherence time of each harmonic is of the order of the pulse duration, a few tens of femtoseconds. The pulse is close to the Fourier limit, i.e., the lower limit for the pulse duration for a given spectral content of the pulse. However the temporal coherence is not constant along the beam profile. In the generation medium, the source term is the harmonic single atom response or dipole. It can be expressed as a superposition of two quantum contributions called "first" and "second" electron trajectories[9]. Each of this contribution to the total dipole has a phase φ with a linear dependence with the IR intensity I : $\varphi=\alpha I$ where α is depending on the electron trajectory. Spatial and temporal variation of I will then lead to an increased spatial divergence and to a spectral broadening of the harmonic. First

trajectory for which α is small will be less divergent and spectrally narrow compared to second trajectory contribution for which α is many times greater.

This intensity dependence of the dipole phase and time dependent ionisation of the medium can affect the pulse length of a single harmonic leading to a small difference from the Fourier limit. The important point is that the harmonic field E can still be described in a deterministic form, using the spectral amplitude A(ω) and phase $\varphi(\omega)$, $E(\omega) = A(\omega)\exp(i\varphi(\omega)$, and this description does not change significantly from one pulse to the next. The spectral phase can in principle be measured using sophisticated frequency resolved optical gating (FROG) techniques.[10]

An interesting feature of high order harmonic generation is the mutual coherence properties of sources generated by two separated beams coming from the same laser chain. This property led to the development of internal frequency conversion interferometer, which has the potential of significantly simplify EUV interferometric devices.[11]. In addition, two consecutive harmonic orders have a stable phase relationship leading in the temporal domain to an attosecond pulse train structure in a similar way to modelocking in infrared lasers. Once this relative phase difference is known, manipulation techniques like EUV chirped mirrors can be developed to minimize the duration of each pulse of this train.

3.2 Applications of High Order Harmonic Coherence

Applications of the coherence properties of high order harmonics have been extensively explored. These include EUV transient grating experiments which are under consideration to explore surface and solid wave dynamics at very high wave vectors.[12] Two harmonic beams crossing at a large angle θ on a surface will generate a fringe pattern of period $\lambda_{HHG}/2\sin(\theta/2)$. If powerful enough, this intensity modulation will excite a wave with an imposed wavevector. The decay of this wave can be followed through the diffraction of a third beam (also coming from an harmonic source) on this transient grating.
Demonstration of coherent or lens-less imaging of nano-system using high order harmonics, has also been demonstrated recently.[13] Numerical reconstruction techniques are required to retreave the object. They not only allow the identification of small details in the object due to use of short wavelength but also allows 3D reconstruction.

It should be also noted that high order harmonics without spectral selection will of course cover a large range of wavelengths and will thus be associated with a very short temporal coherence time. It has been suggested that this property might be useful for the detection of buried defects in EUV lithography masks.[14]if technics similar to the optical coherence tomography (OCT) were developed.

4 COHERENCE OF PLASMA BASED EUV AND SOFT X-RAY LASERS

4.1 General Properties

Plasma based soft X-ray lasers operate in the same spectral range as high order harmonic sources. In these devices, a population inversion is obtained between two levels of highly charged ions in a hot dense plasma. The plasma generation and pumping require a high current and a fast discharge in a capillary or high energy and/or high intensity lasers.[15]